Applied Catalysis B: Environmental 232 (2018) 574–586

Contents lists available at ScienceDirect

Applied Catalysis B: Environmental

journal homepage: www.elsevier.com/locate/apcatb

Novel 3D core-shell structured CQDs/Ag_3PO_4@Benzoxazine tetrapods for enhancement of visible-light photocatalytic activity and anti-photocorrosion

Ning Shao[a], Zhiang Hou[a], Hanxu Zhu[a], Jinnan Wang[a,*], Corvini Philippe François-Xavier[b]

[a] State Key Laboratory of Pollution Control and Resource Reuse & School of the Environment Nanjing University, Nanjing 210023, China
[b] School of Life Sciences, University of Applied Sciences and Arts Northwestern Switzerland, Basel 4132, Switzerland

ARTICLE INFO

Keywords:
3D core-shell structured CQDs/Ag_3PO_4@benzoxazine tetrapods
{110} Facets
Visible-light photocatalytic activity
Anti-photocorrosion
Electrons transfer

ABSTRACT

To improve the visible-light photocatalytic activity and anti-photocorrosion of Ag_3PO_4, novel 3D core-shell CQDs/Ag_3PO_4 @benzoxazine tetrapods with more exposure of {110} facets of Ag_3PO_4 has been successfully synthesized for the first time by electrochemical oxidation, chemical precipitation and molecular self-assembly reaction. In CQDs/Ag_3PO_4@benzoxazine tetrapods, CQDs could not only induce more photocarrier generation from high-energy facets of Ag_3PO_4 tetrapods but also accelerate the electrons transfer from conduction band of Ag_3PO_4 tetrapods to the bottom of conduction band of CQDs. Furthermore, silver amine complex could act as a bridge for the photo-electrons flowing from core to shell, which is beneficial to the subsequent free radical chain reaction. In addition, the 3D core-shell structure decreased the solubility of Ag_3PO_4. UV–vis DRS, indicating that the band gap of CQDs(0.38%)/Ag_3PO_4 @benzoxazine (1.65 eV) was far less than that of Ag_3PO_4 tetrapods (2.0 eV) and traditional Ag_3PO_4 (2.45 eV). Moreover, the photocurrent tests showed that CQDs(0.38%)/Ag_3PO_4@benzoxazine had perfect drift ability of generated photocarriers. Accordingly, the CQDs(0.38%)/Ag_3PO_4@benzoxazine tetrapods exhibited excellent visible-light photocatalytic activity and anti-photocorrosion performance. More than 93% of Methylorange and rhodamine B could be photodegraded within 16 min and 10 min over CQDs(0.38%)/Ag_3PO_4@benzoxazine tetrapods, respectively. Even after 9 cycles, CQDs(0.38%)/Ag_3PO_4@benzoxazine could still remain 95% removal rate of sulfamethoxazole (SMX) with 10 min. Through recycling catalytic experiments and photodegradation pathway explore of SMX, the CQDs(0.38%)/Ag_3PO_4@benzoxazine composite suggest its great mineralization capability on sulfonamide antibiotics. The free radicals trapping experiments demonstrated that the holes photoinduced were the main active oxidizing species which played the dominant role in the photocatalytic process. Thus, CQDs(0.38%)/Ag_3PO_4@benzoxazine is a promising visible-light responses catalyst for photodegradation of organic pollutants in the environmental protection.

1. Introduction

In the past few years, much progress has been made in developing visible light responsive photocatalysts, especially for the Ag-based photocatalysts [1–4], Bi-based photocatalysts [5–9], N or S doped TiO_2 photocatalysts [10–12]. Among those photocatalysts, silver orthophosphate (Ag_3PO_4) had attracted considerable attention since it was discovered by Yi et al. in 2010 [13]. It has demonstrated that Ag_3PO_4 not only has the highest quantum efficiency of 90% at the wavelengths longer than 420 nm [1], but also exhibits extremely high photo-oxidative capabilities for O_2 evolution from water splitting as well as organic dye decomposition under visible light irradiation. However, the unwanted and uncontrolled photocorrosion of Ag_3PO_4 seriously inhibited its widely application in practice [14]. Generally, photocorrosion of Ag_3PO_4 is mainly resulted from its slight solubility ($Ksp = 1.6 \times 10^{-16}$) and energy-band structure [15,16]. Since the conduct band (CB) energy of Ag_3PO_4 (0.45 ev) is higher than the reduced potential of H_2O/H_2, photogenerated electrons of CB cannot be captured by H_2O if there are not any other scavengers in the solution [17]. Consequently, the electrons is obliged to be adopted by the Ag^+ released from the crystal lattice of Ag_3PO_4, which leads to the deposition of Ag° on the surface of photocatalysts ($4Ag_3PO_4 + 6H_2O + 12h^+ + 12e^- \rightarrow 12Ag + 4H_3PO_4 + 3O_2$). This process sharply decreases its photocatalytic activity, stability and lattice constucture. Thus, it is still a huge challenge to develop an ingenious way to overcome the photocorrosion of Ag_3PO_4 as well as promote its catalytic performance.

Since microstructure was considered as an important factor which

* Corresponding author.
E-mail address: wjnnju@163.com (J. Wang).

https://doi.org/10.1016/j.apcatb.2018.03.085
Received 26 January 2018; Received in revised form 13 March 2018; Accepted 24 March 2018
Available online 26 March 2018
0926-3373/

could influence the photocatalytic activity of Ag_3PO_4, various microstructures of Ag_3PO_4 such as cubes, rhombic dodecahedrons and tetrahedroids were successfully synthesized [13,18]. Ye et al.[13] demonstrated that Ag_3PO_4 rhombic dodecahedrons with the active {110} facets exposed had a much higher activity than the cubes with the exposed {100} facets for the degradation of rhodamine B (RhB). Teng et al. also reported that Ag_3PO_4 tetrapods with the high-energy{110} facets exposed have a higher photocatalytic activity than the irregular one [19–21]. In addition, Wang et al. had discovered that Ag_3PO_4 crystals with the exposed {111} facets could improve photocatalytic properties [22,23]. To the best of our knowledge, although the limited crystals control could enhance photocatalytic capability in a certain degree, photocorrosion for Ag_3PO_4 still remained to be resolved. On the other hand, great efforts has been made to improve and optimize their photoelectric and photocatalytic properties by modification of Ag_3PO_4 such as semiconductor coupling [15,24,25] and polymer composites [26,27]. Our previous work also prepared 3D Ag_3PO_4/MoS_2@TiO_2(3.5 wt%) with high photocatalytic activity and stability, and further demonstrated that MoS_2@TiO_2 heterostructure and vertical few-layer MoS_2 could accelerate separation of electron-hole pairs [28]. Therefore, it is expected to improve the photocatalytic performance by simultaneously microstructure control and modification of Ag_3PO_4 in synthesis process.

Among the modifying materials, carbon quantum dots (CQDs) are considered as a new type of quantum dots due to its unique optical and electronic properties. Notably, due to possessing excellent upconversion photoluminescence (UPCL), lower-energy light (visible or near-infrared light from 500 to 1000 nm) can be converted to higher-energy light (ultraviolet or visible light from 325 to 425 nm) via the multiple photon absorption property of CQDs [29]. Thus, CQDs enables could improve the utilization of the visible and near-infrared spectrum of sunlight. In addition, as either electron acceptor or electron donor, CQDs possess the photo-induced electron transfer properties which can offer exciting opportunities for light energy conversion [30,31]. Thus, the combination between crystal control of Ag_3PO_4 and modification with CQDs during the crystal growth process could improve the antiphotocorrosion and photocatalytic activity of Ag_3PO_4. To our best of knowledge, it is the first time to synthesize a three-dimensional CQDs/Ag_3PO_4 tetrapodas.

On the other hand, many researchers have reported that core-shell structure could improve the stability of catalysts. Various materials including graphene, polymer gel and g-C_3N_4 were tried to coat the catalysts [15,26,27,32–34]. It is worth noting that Cui et al had deeply studied the Ag-based photocatalysts for improving the photocatalytic activity and photostability, including Ag_3PO_4@PANI core@shell hybrid, Ag_3PO_4@g-C_3N_4 hybrid core@shell composite, Ag@AgCl QDs sensitized Bi_2WO_6, 3D Ag_3PO_4-graphene hydrogel and 3D graphene hydrogel-AgBr@rGO [15,27,35–37]. These researches mentioned above provided us important inspiration on the design of 3D core-shell structure for photocatalysts. Among them, polymer gels utilized as structured reaction vessels and reusable photocatalysts arouse people's interests and attention in recent years [38]. Hu et al. successfully synthesized the benzoxazine monomer with the structure of an oxazine ring attached to a benzene ring which could form physical gels by the intermolecular bond [39,40]. Due to high active surface area and excellent diffusion properties, benzoxazine monomer could possess immense molecular design flexibility [41,42]. Besides, benzoxazine monomer coated on catalyst which formed core-shell structure could facilitate molecules to access the active sites located within composites and reduce the residence time of molecules in catalysts with fast molecular mass transport, resulting in enhancing reaction rates and slowing deactivation [43]. Thus, we expect to design a novel 3D CQDs/Ag_3PO_4 tetrapods coated with benzoxazine monomer to efficiently resolve the photocorrosion of Ag_3PO_4.

Based on the conception mentioned above, we have successfully prepared novel 3D core-shell structured CQDs/Ag_3PO_4@benzoxazine composites by molecular self-assembly between 'Ag^+' ions and 'amino groups' of benzoxazine monomers for the first time. Being attributed to synergistic function of Ag_3PO_4 tetrapods, CQDs and benzoxazine monomer, 3D structured CQDs/Ag_3PO_4@benzoxazine shows excellent photocatalytic activity and anti-photocorrosion. In CQDs/Ag_3PO_4@benzoxazine composite, CQDs act as an 'exciter' because of its electron acceptor characteristic, which can activate more photocarrier generation from high-energy facets of Ag_3PO_4 tetrapods by strengthening light absorption and energy conversion via UPCL effect. Meanwhile, CQDs can also accelerate the electrons transfer from conduction band of Ag_3PO_4 tetrapods to the bottom of conduction band of CQDs. Furthermore, the photo-electrons flow to silver amine complex ion which can act as a bridge between core and shell. In addition, the 3D core-shell structure effectively decreased the solubility of Ag_3PO_4. To achieve this objects, our study focuses on the following five aspects: (1) to synthesize 3D core-shell structured CQDs/Ag_3PO_4@benzoxazine via electrochemical oxidation, chemical precipitation and molecular self-assembly approaches; (2) to characterize this novel photocatalyst by using FE-SEM,TEM,XPS,XRD,DRS and Photocurrent test; (3) to test the photocatalytic activity by degradation of Methyl orange (MO) and Rhadamine B (RhB); (4) to evaluate the photocatalytic stability and anti-photocorrosion by degradation of sulfamethoxazole (SMX) ; and (5) to propose the possible photocatalytic degradation pathways and mechanisms.

2. Experimental

2.1. Chemicals

All the chemicals used in the experiment were analytical grade and purchased from Aladdin Corporation (shanghai,China). The graphite rods (99.9%) were supplied by Alfa Aesar Co.Ltd.

2.2. Synthesis of CQDs/Ag_3PO_4@benzoxazine

2.2.1. Synthesis of CQDs

The large-scale synthesis of high-quanlity carbon quantum dots has adopted a direct electrochemical oxidation approach as reported in literatures [44,45]. In brief, graphite rods were used as both the anode and cathode, and ultrapure water was used as an electrolyte without addition of any other chemicals. Then, CQDs was prepared under a direct current density of 45-60 mA cm^{-2} for 120 h with continuous stirring at 120 rpm. Along with the anode graphite rod being corroded, the color of solution gradually became dark-yellow in the reactor. After being filtered by slow-speed quantitative filter paper, the resultant solution was centrifuged (11,000 rpm) for 30 min to separate the precipitated graphite oxide and graphite particles away from the solution. Finally, the solution was dried under vacuum at 60 ℃ to obtain CQDs.

2.2.2. Synthesis of CQDs/Ag_3PO_4 tetrapods

We developed a new method to prepare CQDs/Ag_3PO_4 tetrapods. The samples were synthesized by a simple precipitation reaction system. Typically, certain amount of CQDs was added to 140 ml deionized water (DW) and the CQDs solution was ultrasound for 40 min. Then, 10.4 ml tetrahydrofuran (THF) (the THF/DW volumetric ratios was 0.065/1) was added into the CQDs solution under vigorous stirring. Subsequently, 205 μL of 85 wt% H_3PO_4 and 1.31 g of hexamethylenetetramine (HMT) were introduced into the above mixture. Then, 20 ml of $AgNO_3$ solution (0.47 mol L^{-1}) was added in the reaction system under stirring (100 rpm) for 5 min at 303 K. Finally, the green-yellow precipitation was collected and washed by deionized water and ethanol, dried at 55℃ for 6 h.

2.2.3. Synthesis of benzoxazine monomer

0.025 mmol melamine and 0.125 mol formaldehyde were added into 200 ml of methanol solution (volume ratio of 1:1) in a round-

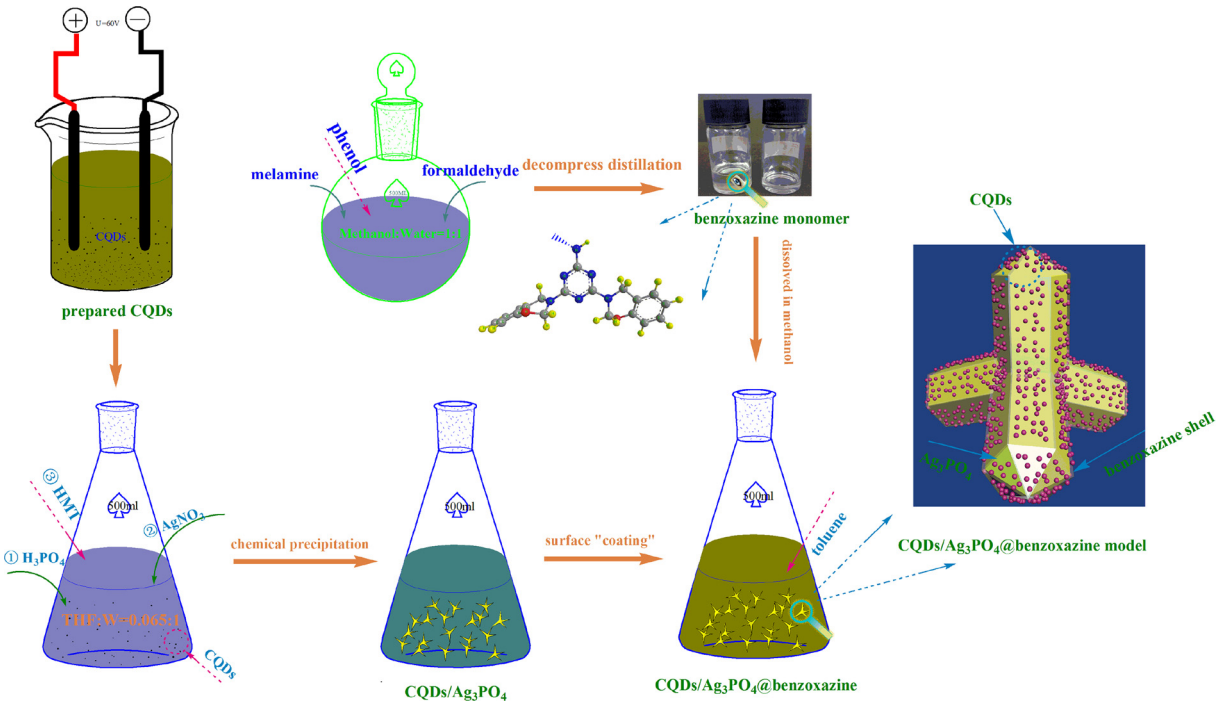

Scheme 1. Schematic of synthesize of CQDs/Ag3PO4@ benzoxazine.

bottom flask at 60 ℃ with magnetic stirring (150 rpm) for 40 min. Then, 0.05 mol phenol was added into the round-bottom flask in water-bath (85℃).After reaction for 6 h, the solvents were removed from the round-bottom flask by decompressing distillation (−0.1 Mpa) at 55 ℃. Finally, benzoxazine monomer with low-viscosity and transparent colorless was obtained.

2.2.4. Synthesize of 3D tetrapods CQDs/Ag_3PO_4@benzoxazine with core-shell structure

0.418 g CQDs/Ag_3PO_4 tetrapods was added into 70 ml toluene, and then mixed with 250 ml of benzoxazine monomer emulsion (0.2864 g L^{-1}). After stirring in water-bath (65 ℃) for 3 h, the products were centrifuged and dried at 80 C for 12 h. Finally, 3D tetrapods CQDs/Ag_3PO_4@benzoxazine with core-shell structure was obtained.

The whole synthesis process is shown in Scheme 1.

2.3. Characterization of CQDs/Ag_3PO_4@benzoxazine

The morphology and microstructure of the samples were characterized by field emission scanning electron microscope (FESEM, S-3400NII, Hitachi, Japan) and transmission electron microscope (TEM, JEOLJEM-200CX, JEOL, Japan). To observe the dispersion of elements on catalysts surface, the EDS mapping images were captured on the atomic resolution analytical microscope (Tecnai G2 F20 S-TWIN, FEI, America). The crystal phases of samples were recorded on the X-ray diffractometer (Cu-kα radiation, X'TRA, Switzerland) in the range of 10–80° (2θ) at a scanning rate of 5° min^{-1}. Furthermore, X-ray photoelectron spectroscopy (XPS, PHI 5000 VersaProbe, UlVAC-PHI, Japan) with an Al-kα X-ray source were used to determined binding energies of Ag, N, C, P and O of CQDs/Ag_3PO_4@benzoxazine. As an important index for measuring photocarrier migration, the photocurrent responses were tested by the electrochemical analyzer (CHI660E, Shanghai, China) with a standard three-electrode configuration. In addition, the UV–vis diffuse reflectance spectra (DRS) were performed on the UV–vis spectrophotometer (UV-3600, Shimadzu, Japan) with an intergrating sphere to evaluate the photosensitivity.

2.4. Photocatalytic activity tests

Photocatalytic degradation of methyl orange (MO) and rhadamine B (RhB) were conducted to evaluate the photocatalytic activity of CQDs/Ag_3PO_4@benzoxazine at 25 ℃. In order to optimize the CQDs content of catalyst, photocatalytic degradation of MO over CQDs/Ag_3PO_4@benzoxazine with various CQDs contents (0.05%–1.15%) were comparatively studied as follows: 0.15 g photocatalyst was added into 500 ml MO aqueous solution (2.5 mg L^{-1}) in XPA-Photochemical Reactor (Xujiang Electromech-anical Plant,Nanjing,China) with 800 w xenon (Xe) arc lamp irradiation. To ensure the dispersion of photocatalyst in solution and adsorption-desorption equilibrium of MO on photocatalysts, all photodegradation solutions were stirred at 120 rpm in the dark for 30 min (Fig. S1). 5 m l suspensions were sampled at a given time interval during the photodegradation experiment, followed by centrifugation (3500 rpm) to separate the photocatalyst. Then, the concentration of MO was determined by the UV–vis spectrophotometer (wavelength = 464 nm).The photocatalytic degradation rate (E%) was calculated according to Eq. (1).

$$E\% = (C_0\text{-}C)/C_0 \times 100\% \quad (1)$$

Where C_0 (mg L^{-1}) is the initial concentration,while C (mg L^{-1}) is the concentration of MO after irradiation at any time. C can be calculated through the corresponding absorbance according to the standard curve.

In addition, in order to evaluate the synergistic effect of CQDs and benzoxazine on improvement of photocatalytic performance, photocatalytic degradation of RhB over CQDs/Ag_3PO_4@benzoxazine and Ag_3PO_4 were comparatively studied as following method: 0.15 g photocatalyst was added into RhB aqueous solution. To ensure the total amount of photocatalyst unchanged during the whole batch photodegradation process, the small amount of precipitation of photocatalyst was recirculated to reactor after each sampling and centrifugation. The detection wavelength for RhB was 553 nm.

2.5. Anti-photocorrosion evaluation

In order to evaluate the anti-photocorrosion of CQDs/Ag_3PO_4@ benzoxazine, 9 cycling runs of photocatalytic degradation of

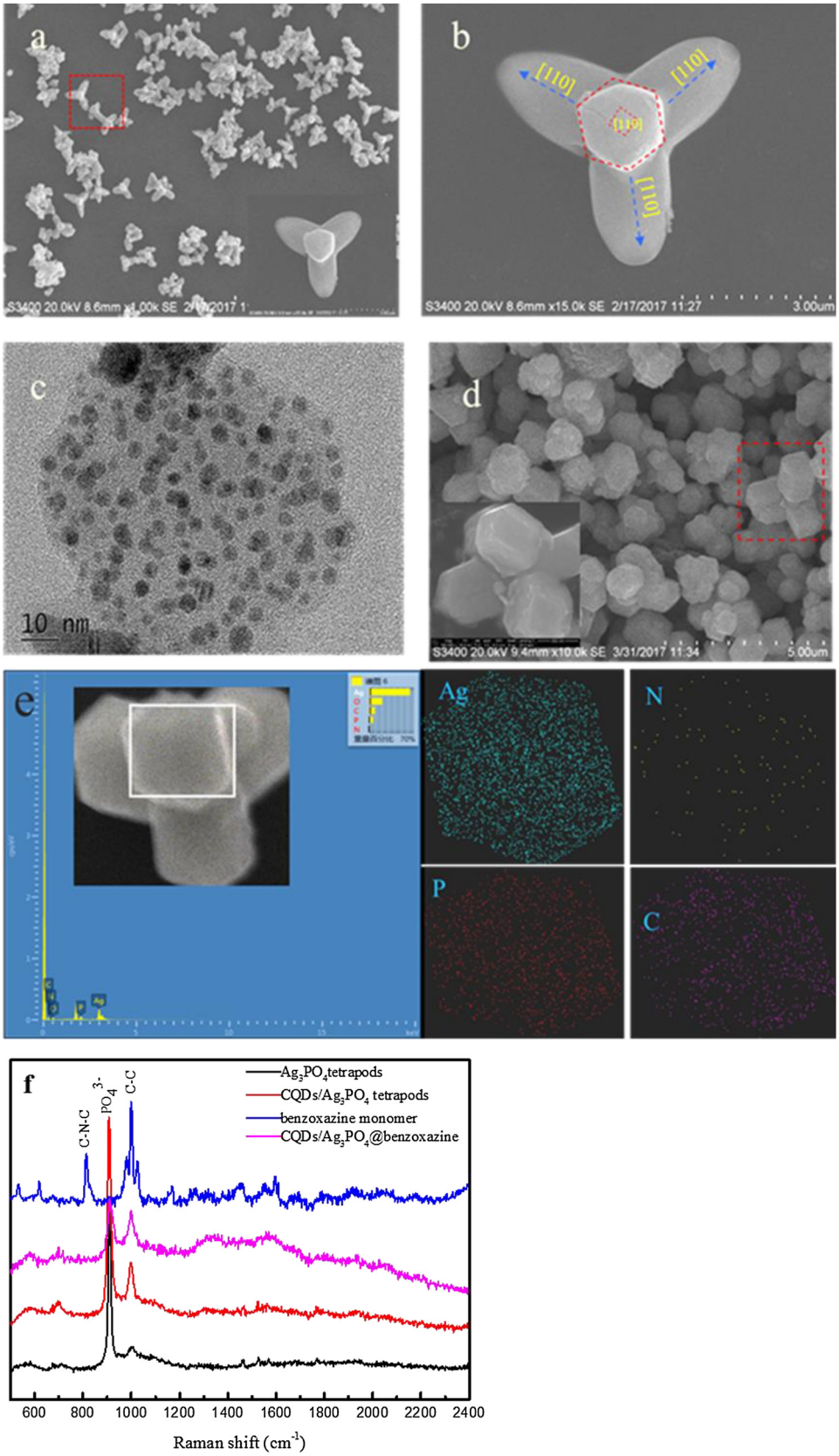

Fig. 1. SEM images of (a) CQDs/Ag_3PO_4, (b) FE-SEM images of CQDs/Ag_3PO_4 and [110] crystal growth direction of Ag_3PO_4 tetrapods, (c) TEM images of CQDs/Ag_3PO_4, (d) FE-SEM images of CQDs/Ag_3PO_4@benzoxazine and (e) the corresponding energy dispersive spectrometer (EDS) of CQDs(0.38%)/Ag_3PO_4@benzoxazine, (f) Raman spectra of Ag_3PO_4 tetrapods, CQDs/Ag_3PO_4 tetrapods, benzoxazine monomer and CQDs/Ag_3PO_4@benzoxazine.

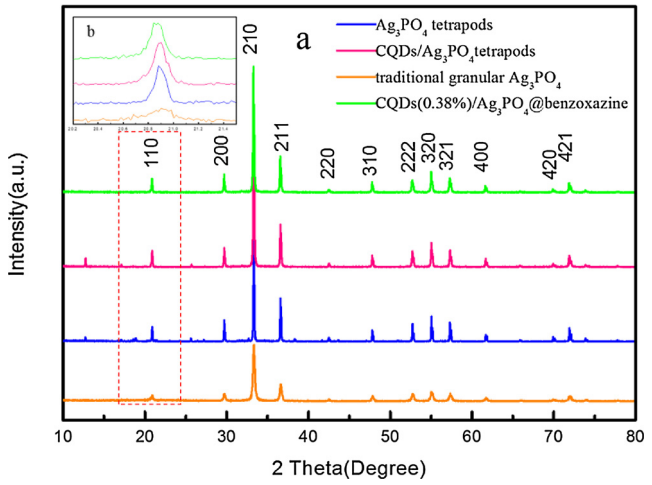

Fig. 2. XRD patterns of Ag_3PO_4 tetrapods, CQDs(0.38%)/Ag_3PO_4 tetrapods, traditional granular Ag_3PO_4 and CQDs(0.38%)/Ag_3PO_4@benzoxazine.

sulfamethoxazole (SMX) were conducted as follows: In XPA-Photochemical Reactor (Xujiang Electromech-anical Plant, Nanjing, China) with a 800 w xenon (Xe) arc lamp irradiation, 0.10 g CQDs/Ag_3PO_4@benzoxazine was added into 500 mL of SMX solution (5 mg L^{-1}). 5 mL suspensions were sampled at a given time interval, followed by centrifugation at 3500 rpm to separate the photocatalyst. Then the concentration of SMX were analyzed by using high performance liquid chromatography (HPLC, Agilent, America) in the process of the reaction. The intermediate products of SMX during the photocatalytic process were detected by high performance liquid chromatography coupled with time-of-flight mass spectrometry detection (HPLC–TOFMS, Agilent 1290 Infinity LC/6460 QQQ MS) in positive polarity. The operating conditions of HPLC and HPLC-TOFMS are listed in Table S1.

2.6. Photocatalytic mechanism of CQDs(0.38%)/Ag_3PO_4@benzoxazine

In order to further illustrate the photocatalytic mechanism, tapping free radicals experiments were conducted to confirm the reactive oxidative species. The active species generated in the photocatalytic system could be trapped by ethylenediamine tetraacetic acid disodium salt (EDTA-2Na), tert-butanol (tBuOH) and p-benzoquinone, by which we could preliminarily demonstrate the main reactive oxidative species. Thus, EDTA-2Na (5 mM), tBuOH (5 mM) and p-benzoquinone (5 mM) were respectively added into MO (5 mg L^{-1}) and RhB (5 mg L^{-1}) solution before photodegradation reaction. And the photodegradation conditions were as same as Section 2.4.

3. Results and discussion

3.1. Characterization of CQDs/Ag_3PO_4@benzoxazine

3.1.1. SEM and TEM analysis

The morphologies and microstructures and compositions of the products were characterized by FESEM and TEM. It is observed that the CQDs/Ag_3PO_4 tetrapods has four branches with {110} facets exposed (Fig. 1a, b). These branches are microrods with an average diameter of 1.5 μm and a length of 2 μm. Notably, the high-quanlity carbon quantum dots (2–5 nm) are homogeneously decorated on the surface of Ag_3PO_4 crystals (Fig. 1c). To our best knowledge, this is the first time to directly synthesized tetrapod-like silver orthophosphate with uniform dispersion of high-quanlity carbon quantum dots. Being attributed to the nano-scale property, C-dots possessed high photocatalytic activity under visible irradiation so that it showed great potential for high-efficiency complex catalyst design [46]. After coating benzoxazine on CQDs/Ag_3PO_4 tetrapods, surface of CQDs/Ag_3PO_4@benzoxazine was covered by a layer of transparent film and becomes rough. In the process of coating benzoxazine, due to the existence of unbonded electrons in 'N' atoms, Ag^+ of Ag_3PO_4 and amino groups of benzoxazine monomers could form silver amine complex compound. Such molecular self-assembly process led to formation of the core–shell CQDs/Ag_3PO_4@benzoxazine composites (Fig. 1d). In the Raman spectra (Fig. 1f), the pure Ag_3PO_4 tetrapods and CQDs/Ag_3PO_4 tetrapods present an intense sharp band at 910 cm^{-1} ascribed to the PO_4^{3-} symmetric stretching vibrations [47]. Meanwhile, the peaks located at 813 cm^{-1} correspond to C—N—C symmetric stretch vibrations of benzoxazine monomers. Additionally, the band near 1000 cm^{-1} is ascribed to C—C stretching vibration of benzoxazine ring. What's more, the characteristic peak of C—N—C symmetric stretch vibrations disappears in CQDs/Ag_3PO_4@benzoxazine composites, which can further confirm the existence of coordination interaction between Ag^+ ions on the surface of Ag_3PO_4 and amino groups of the benzoxazine monomers to form silver amine complex compound [48]. In addition, X-ray spectrometry (EDS) also confirms the existence of 'N', 'C', 'Ag', 'P' and 'O' in 3D CQDs/Ag_3PO_4@benzoxazine (Fig. 1e).

3.1.2. X-ray diffraction (XRD)

The crystal structure and phase composition of CQDs/Ag_3PO_4@benzoxazine, traditional granular Ag_3PO_4, Ag_3PO_4 tetrapods and CQDs/Ag_3PO_4 tetrapods were analyzed by XRD. In the XRD pattern of CQDs/Ag_3PO_4@benzoxazine, all of the diffraction peaks can be clearly assigned to the cubic phase of Ag_3PO_4 (JCPDS card no.06-0505) (Fig. 2a). The diffraction peaks at 21.7°, 29.7°, 33.3°, 36.5°, 42.49°, 47.8°, 52.6°, 54.9°, 57.2°, 61.8°and 71.8° are respectively ascribed to the (110), (200), (210), (211), (220), (310), (222), (320), (321), (400) and (421) diffraction phases of Ag_3PO_4 tetrapods. Notably, compared to traditional granular Ag_3PO_4, it shows stronger intensity of (110) phase which indicates that CQDs/Ag_3PO_4 tetrapods exposes more {110} facets (Fig. 2b). Based on JADE crystal phase analysis for XRD data, the peak area ratio of (110)/(210) increased from 0 to 6% and the peak intensity ratio of (110)/(210)increased from 0 to 10% in CQDs/Ag_3PO_4 tetrapods compared with traditional granular Ag_3PO_4 (Fig. S5). Generally, increasing the percentage of high-energy surfaces of Ag_3PO_4 could improve the photocatalytic properties in applications [13]. It must be noted that although increasing high-energy {110} facets can enhance the catalytic activity of Ag_3PO_4, the (210) facet still plays an important role in photocatalytic reaction. In addition, although benzoxazine coated on the CQDs/Ag_3PO_4 tetrapods and formed the silver amine complex compound (Fig. 1d), the XRD spectrogram demonstrates that the crystal structure and phase of Ag_3PO_4 keep unchanged during the whole preparation process of CQDs/Ag_3PO_4@benzoxazine.

3.1.3. X-ray photoelectron spectroscopy (XPS)

The elemental compositions of CQDs(0.38%)/Ag_3PO_4@benzoxazine and the valence states of Ag were further analyzed by XPS. As discerned from the XPS spectra of Ag 3d (Fig. 3a), two individual peaks appeared at 366.30 eV and 372.3 eV respectively ascribed to $3d_{3/2}$ and $3d_{5/2}$ of typical Ag^+ [49,50]. In the N 1s spectra (Fig. 3c), peaks with three binding energies appeared in sample, which were assigned to C—N═C, C—N—C and unsaturated amino groups C—N—H (398.7 eV). According to the previous literatures [40,51], there was strong interaction between Ag^+ from surface of Ag_3PO_4 tetrapods and amino groups, which also confirm the formation of silver amine complex compound as described in Fig. 1d. The characteristic peak (P 2p) of at 131.6 eV (Fig. 3d) corresponds to P^{5+} according to the previous literatures [50]. In addition, the O 1 s binding energy peak (360.64 eV) shown in Fig. 3e suggests the existence of O^{2-} in the composite [52]. Thus, the binding energy of elements in CQDs(0.38%)/Ag_3PO_4@benzoxazine composite (Fig. 3f) are well consistent with the results of EDS analysis (Fig. 1e). In addition, based on an atom slab model, the concave microcrystals with uniform dispersion are obtained by preferential overgrowth along

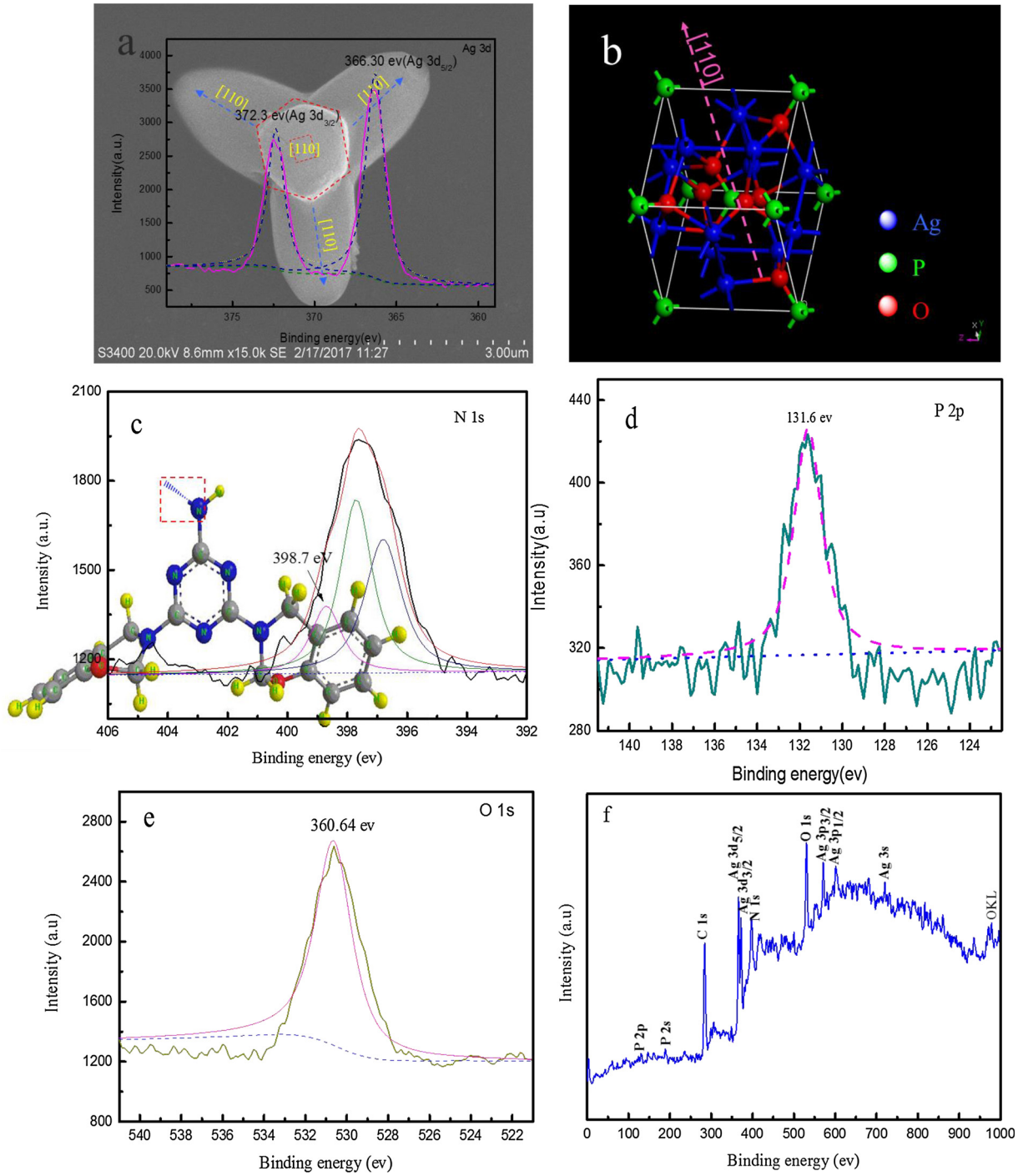

Fig. 3. XPS spectra of the CQDs(0.38%)/Ag_3PO_4@benzoxazine composite: (a) Ag 3d, (b) relaxed geometries for the {110} surfaces of Ag_3PO_4 based on a atom slab model, (c) N 1s, (d) P 2p, (e) O 1s and (f) survey spectrum.

[110] directions of seeds (Fig. 3b). Such microcrystals can be clearly observed by Fig. 3a inset.

3.1.4. UV/vis Diffuse reflectance spectrum

UV–vis DRS is commonly used to measure the band gaps of semiconductors, which can be used to evaluate their generation capability of photocarrier. In order to comparatively study the distinct photocatalytic performance of CQDs(0.38%)/Ag_3PO_4@benzoxazine with other Ag_3PO_4 based photocatalysts, we prepared Ag_3PO_4 tetrapods and CQDs(0.38%)/Ag_3PO_4 as comparisons. As expected, the absorption intensity of 3D CQDs(0.38%)/Ag_3PO_4@benzoxazine composite is about four times higher than that of pure Ag_3PO_4 tetrapods at the range of 520–800 nm wavelength (Fig. 4a), indicating that CQDs(0.38%)/Ag_3PO_4@benzoxazine can make full use of visible light sources during the process of photodegradation pollutants. Such high light absorption intensity might be attributed to the internal synergistic effects between Ag_3PO_4, CQDs and benzoxazine. On one hand, just like 'ignition plug' in the 'motor', CQDs could act as exciter in CQDs(0.38%)/Ag_3PO_4@benzoxazine due to its distinct properties involving the effective absorbance of solar light, tunable photoluminescence (PL), infrared-responsive up-converted photoluminescence (UCPL) and unique photoinduced electron transfer [53]. Accordingly, the CQDs increased the light quantum efficiency of Ag_3PO_4 tetrapods. On the other hand, The intermolecular bond between benzoxazine gels shell and Ag_3PO_4

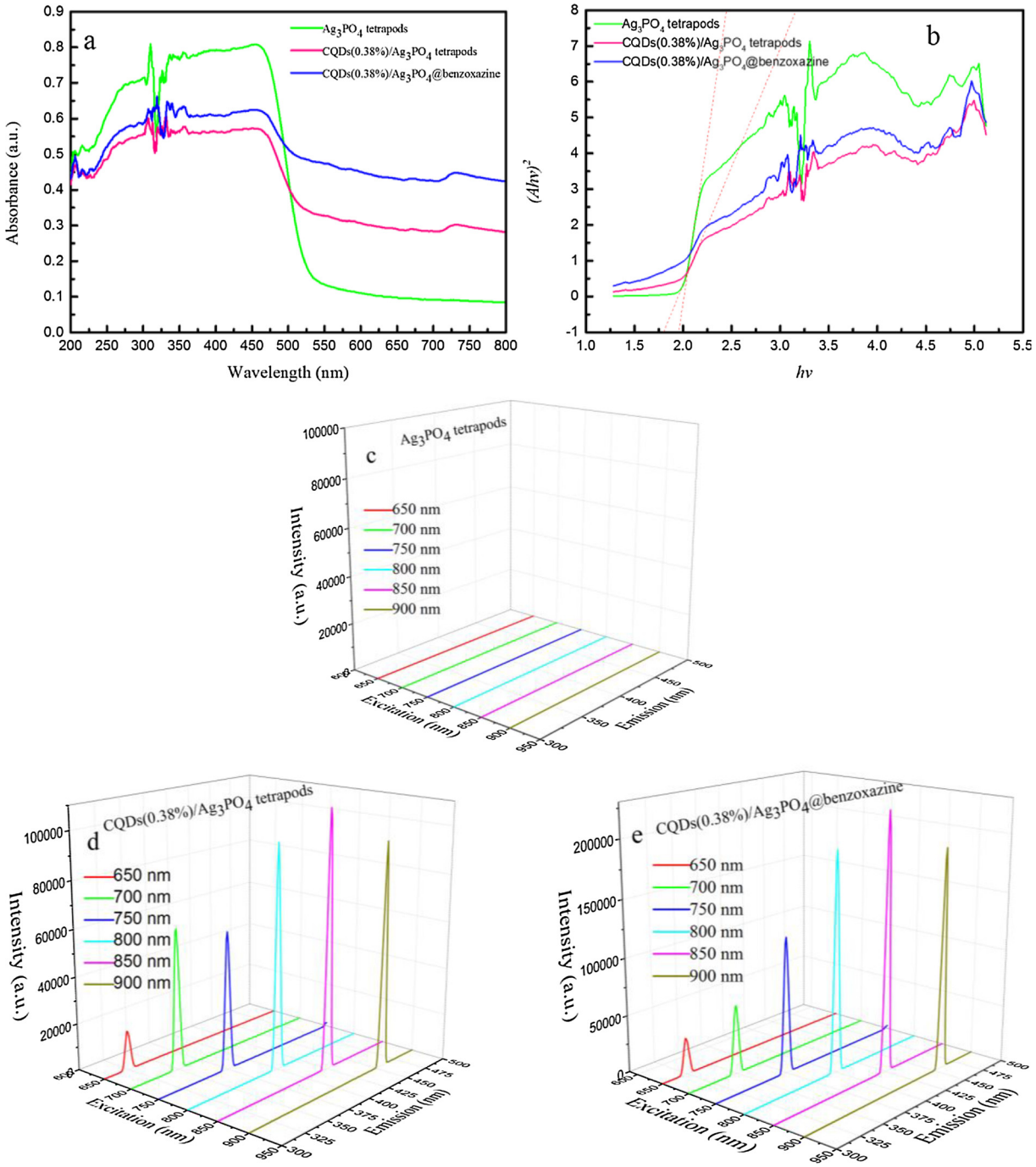

Fig. 4. (a) UV–vis DRS of Ag_3PO_4 tetrapods, CQDs(0.38%)/Ag_3PO_4 and CQDs(0.38%)/Ag_3PO_4@benzoxazine, (b) the corresponding Kubelka-Munk transformed reflectance spectra determines the bandgap values for the photocatalysts. UPCL spectra of (c) blank-Ag_3PO_4 tetrapods, (d) CQDs(0.38%)/Ag_3PO_4 tetrapods and (e) CQDs(0.38%)/Ag_3PO_4@benzoxazine under visible/near infrared excitation.

core could act as a bridge which promoted the molecular mass transport so as to facilitating molecules to contact the active sites located on the surfaces of Ag_3PO_4, especially on {110} facets. According to the unique photoinduced electrons transfer effect of CQDs and Yue et al. research [40], the photogenerated electrons in the conduction band (CB) of Ag_3PO_4 under visible light irradiation could transfer to the silver amine complex ion, which is beneficial to the chain reaction of free radicals. Thus, CQDs and benzoxazine shell synergistically promoted the separation of electron-hole pairs, resulting in a higher absorption intensity of CQDs(0.38%)/Ag_3PO_4@benzoxazine. Interestingly, due to the UCPL effect of CQDs (Fig. 4d and e), the CQDs(0.38%)/Ag_3PO_4@benzoxazine have relatively lower absorption intensity in the range of 250–450 nm wavelength. Based on the Fig. 5a, the band gap of CQDs (0.38%)/Ag_3PO_4 @benzoxazine can be calculated (1.65 eV) (Fig. 5b), which is far less than that of Ag_3PO_4 tetrapods (2.0 eV) and traditional Ag_3PO_4 (2.45 eV) reported in previous literatures [54].

3.2. Photocatalytic degradation activity tests

3.2.1. Photocatalytic degradation of MO and RhB

To confirm the optimal content of CQDs in composite, photocatalytic degradation of MO over CQDs/Ag_3PO_4@benzoxazine with various CQDs content were conducted under visible light irradiation. About 95% of MO is photodegraded within 16 min over CQDs(0.38%)/

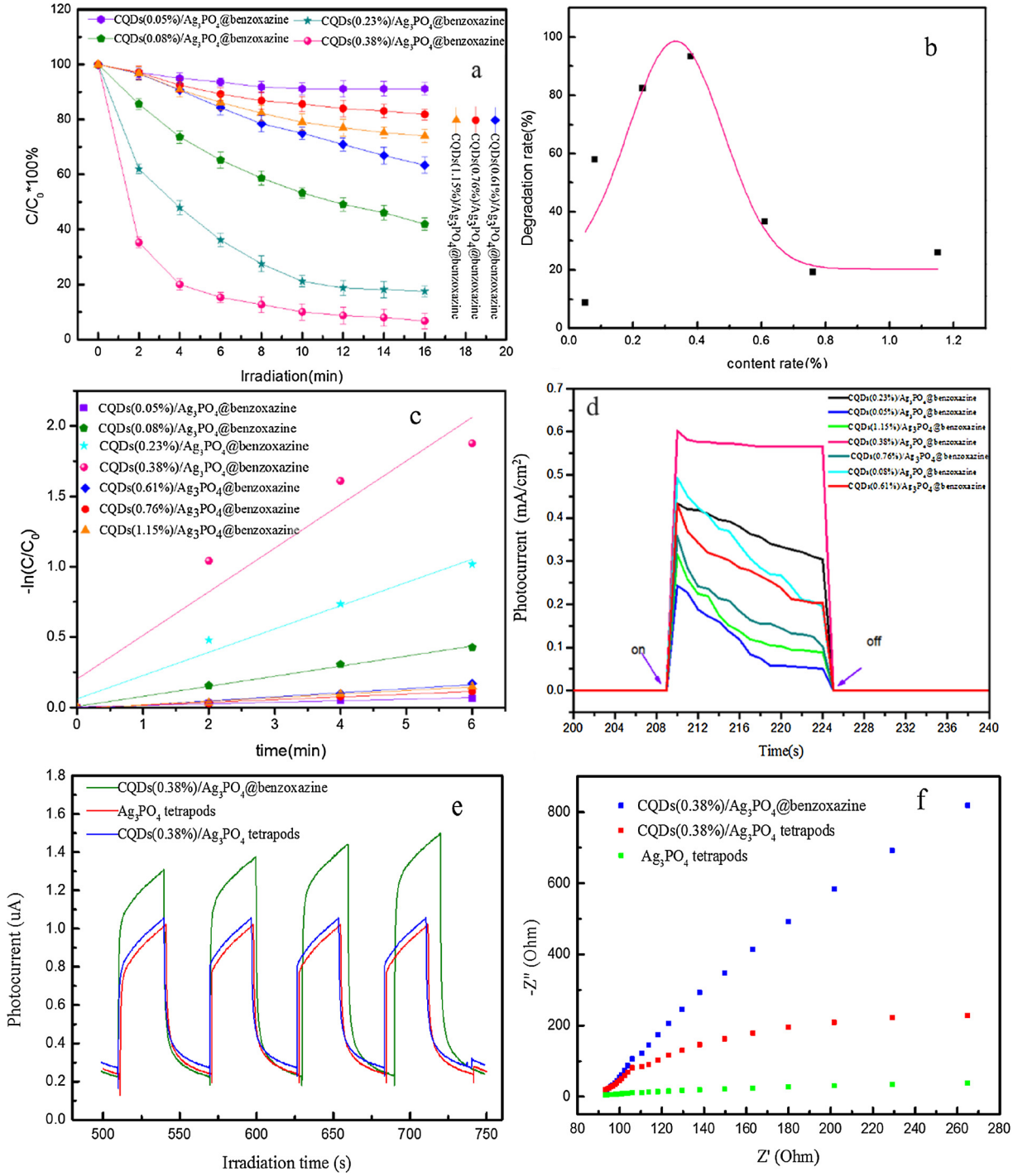

Fig. 5. (a) Photocatalytic degradation of MO over CQDs/Ag_3PO_4@benzoxazine composites with different CQDs contents, (b) the normal distribution curve of photodegradation rate of MO over CQDs/Ag_3PO_4@benzoxazine composites with different CQDs contents, (c) pseudo-first-order kinetic model first the degradation kinetic curves of MO, (d) photoluminescence spectra of CQDs/Ag_3PO_4@benzoxazine composites with different mass fraction, (e) Photocurrent response for the pure Ag_3PO_4 tetrapods, CQDs(0.38%)/Ag_3PO_4 tetrapods and CQDs(0.38%)/Ag_3PO_4@benzoxazine composites, (f) Electrochemical impedance spectroscopy (EIS) Nyquist plots of the sample electrodes of the pure Ag_3PO_4 tetrapods, CQDs(0.38%)/Ag_3PO_4 tetrapods and CQDs(0.38%)/Ag_3PO_4@benzoxazine composite.

Ag_3PO_4@benzoxazine, showing excellent catalytic activity (Fig. 5a). The highest kinetic rate constant of catalyst with 0.38% content of CQDs (0.3100 min^{-1}) is observed, which is 28.5, 14.6 and 11.2 times as much as that of catalyst with 0.05%, 0.76% and 1.15% content of CQDs, respectively (Table 1). More importantly, 92% of the total organic carbon (TOC) of MO could be removed over CQDs(0.38%)/Ag_3PO_4@benzoxazine at the same time (Fig. S4a), showing excellent mineralization ability. Interestingly, the plots of MO photodegradation rate vs. CQDs content in composites present a normal distribution curve (Fig. 5b). When the mass fraction of CQDs is relatively low, such as 0.05%, the photodegradation rate of MO is below 10%. Generally, the photocatalytic process included solar absorption, charge separation and catalytic conversion. Although the benzoxazine shell of Ag_3PO_4 @ benzoxazine reduced the photocorrosion of Ag_3PO_4, solar adsorption was inhibited in a certain degree, resulting in a lower photocatalytic activity compared with pure Ag_3PO_4 tetrapods. Meanwhile, level

Table 1
The pseudo-first-order kinetic equations,rate constants (k) and regression coefficients (R^2) of photocatalytic degradation of MO over CQDs/Ag_3PO_4@benzoxazine composites with various CQDs content.

Series	photocatalyst	The first order kinetic equation	K (min^{-1})	R^2
1	CQDs(0.05%)/Ag_3PO_4@benzoxazine	$-\ln(C/C_0) = 0.0109\,t$	0.0109	0.966
2	CQDs(0.08%)/Ag_3PO_4@benzoxazine	$-\ln(C/C_0) = 0.0715\,t$	0.0715	0.995
3	CQDs(0.23%)/Ag_3PO_4@benzoxazine	$-\ln(C/C_0) = 0.1653\,t$	0.1653	0.996
4	CQDs(0.38%)/Ag_3PO_4@benzoxazine	$-\ln(C/C_0) = 0.3100\,t$	0.3100	0.891
5	CQDs(0.61%)/Ag_3PO_4@benzoxazine	$-\ln(C/C_0) = 0.0288\,t$	0.0288	0.964
6	CQDs(0.76%)/Ag_3PO_4@benzoxazine	$-\ln(C/C_0) = 0.0195\,t$	0.0195	0.987
7	CQDs(1.15%)/Ag_3PO_4@benzoxazine	$-\ln(C/C_0) = 0.0255\,t$	0.0255	0.978

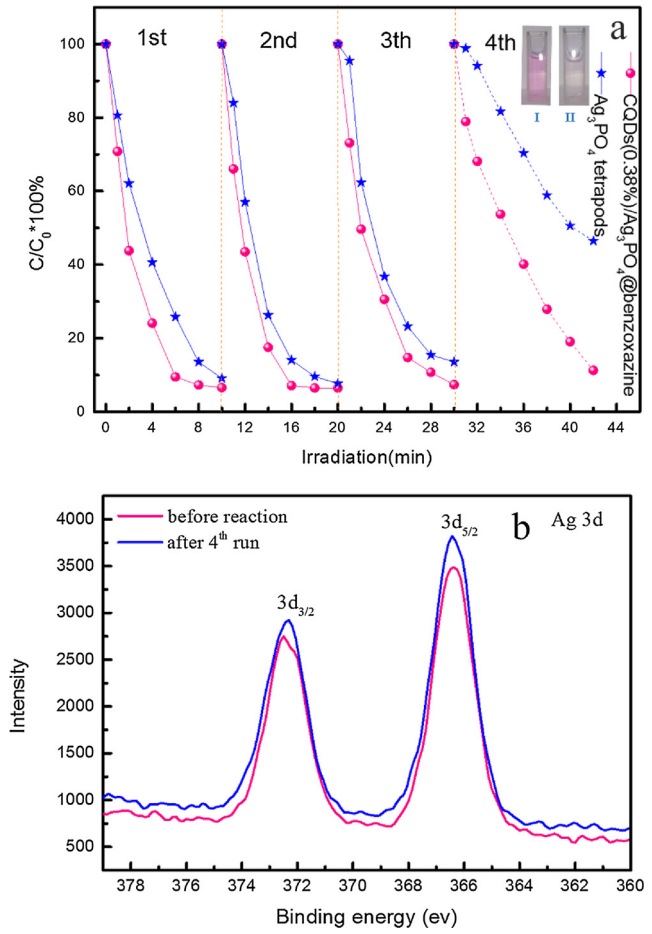

Fig. 6. (a) Cycling runs of Ag_3PO_4 tetrapods and CQDs(0.38%)/Ag_3PO_4@benzoxazine for photodegradation of RhB [inset (I) and (II) show the color of RhB at the 4th recycling photodegradation over Ag_3PO_4 tetrapods and CQDs (0.38%)/Ag_3PO_4@benzoxazine, respectively]; (b) Ag 3d XPS spectra of CQDs (0.38%)/Ag_3PO_4@benzoxazine before and after 4th recycling photodegradation of RhB.

energy of visible light captured by low content of CQDs is not high enough to activate the migration of electrons from the conduction band of Ag_3PO_4 tetrapods under visible light irradiation, therefore the photocatalytic activities was hindered by electron-hole recombination. On the other hand, excess of incorporation of CQDs (e.g. 0.61%, 0.76% and 1.15%) decreased the MO degradation, suggesting that more MO and free radicals adsorbed by CQDs might occupy the active sites of catalyst which inhibited the transformation of photogenerated electrons [55]. In addition, high content of CQDs in composite could absorb the emission energy from themselves so as to lower energy transformation to the CQDs/Ag_3PO_4@benzoxazine. Therefore, there is an optimal content of CQDs in the CQDs/Ag_3PO_4@benzoxazine composite. In order to prove this assumption, the drift ability of generated photocarriers were determined by photocurrent tests. As expected, CQDs(0.38%)/Ag_3PO_4 @benzoxazine showed the highest photocurrent intensity and the most steady intensity tends. Furthermore, according to Cui's research method [56–58], the photocurrent response and electrochemical impedance spectroscopy for various photocatalysts were comparatively studied (Fig. 1e and f). The results demonstrated that CQDs(0.38%)/Ag_3PO_4 @ benzoxazine owned more stronger photocurrent response and lower electrochemical impedance value than CQDs(0.38%)/Ag_3PO_4 tetrapods and pure Ag_3PO_4 tetrapods, which also confirmed that the introduction of CQDs and benzoxazine could promote photogenerated charge separation in CQDs(0.38%)/Ag_3PO_4 @benzoxazine composite.

In order to comparatively study the photocatalytic activities of Ag_3PO_4 tetrapods and CQDs(0.38%)/Ag_3PO_4@benzoxazine composite, successive batch experiments of RhB photodegradation over these two catalysts were conducted. It is observed that the photodegradation rate of RhB by pure Ag_3PO_4 tetrapods declined significantly with the increase of recycles (Fig. 6a). Due to the photocorrosion of Ag_3PO_4 ($4Ag_3PO_4 + 6H_2O + 12\,h^+ + 12e^- \rightarrow 12\,Ag + 4H_3PO_4 + 3O_2$), the photodegradation rate of RhB decreased more than 40% after 4 recycles. On the contrary, CQDs(0.38%)/Ag_3PO_4@benzoxazine still remained excellent photocatalytic activity and stability even after 4 recycling use, which were in accordance with the results of photocurrent tests and Ag 3d XPS analysis. To further confirm the valence states of Ag in composite after photocatalytic reaction, we contrasted the XPS spectra of CQDs(0.38%)/Ag_3PO_4@benzoxazine before and after 4 recycling use. Peaks of Ag $3d_{5/2}$ and $3d_{3/2}$ of Ag^+ (Ag_3PO_4 tetrapods) show no obvious shift after photocatalytic reaction, suggesting the unchanged valence states of Ag^+ [28]. In addition, about 90% of TOC of RhB could be removed over CQDs(0.38%)/Ag_3PO_4@benzoxazine in photocatalytic experiments (Fig. S4b), also showing an excellent mineralization ability.

3.3. Anti-photocorrosion evaluation

To evaluate the potential of CQDs(0.38%)/Ag_3PO_4@benzoxazin in the practical application, the successive batch degradation rate of SMX was tested. As a typical antibiotic with wide application, SMX has been frequently detected in environment, which has aroused people's attention [59–61]. Furthermore, due to its negligible light absorption at wavelengths above 320 nm, SMX was considered as an ideal target organic pollutant to investigate photocatalytic properties of visible-light responsive photocatalysts [62]. Interestingly, about 35% of SMX was adsorbed by CQDs(0.38%)/Ag_3PO_4@benzoxazine in the dark within 30 min (Fig. 7a). Such high equilibrium adsorption capacity for SMX might be attributed to 3D structure of CQDs(0.38%)/Ag_3PO_4@ benzoxazine and similar molecular structure of benzoxazine and sulfamethoxazole. Generally, 3D structure of catalyst with high specific surface area (129 m^2/g) could provide more adsorption sites (Fig. S3). Meanwhile, similar molecular structure of benzoxazine and SMX led to a match effect which was also beneficial to adsorption. Accordingly, excellent adsorption capacity of CQDs(0.38%)/Ag_3PO_4@benzoxazine for SMX promoted the photocatlytic degradation process.

Notably, CQDs(0.38%)/Ag_3PO_4@benzoxazine exhibits excellent

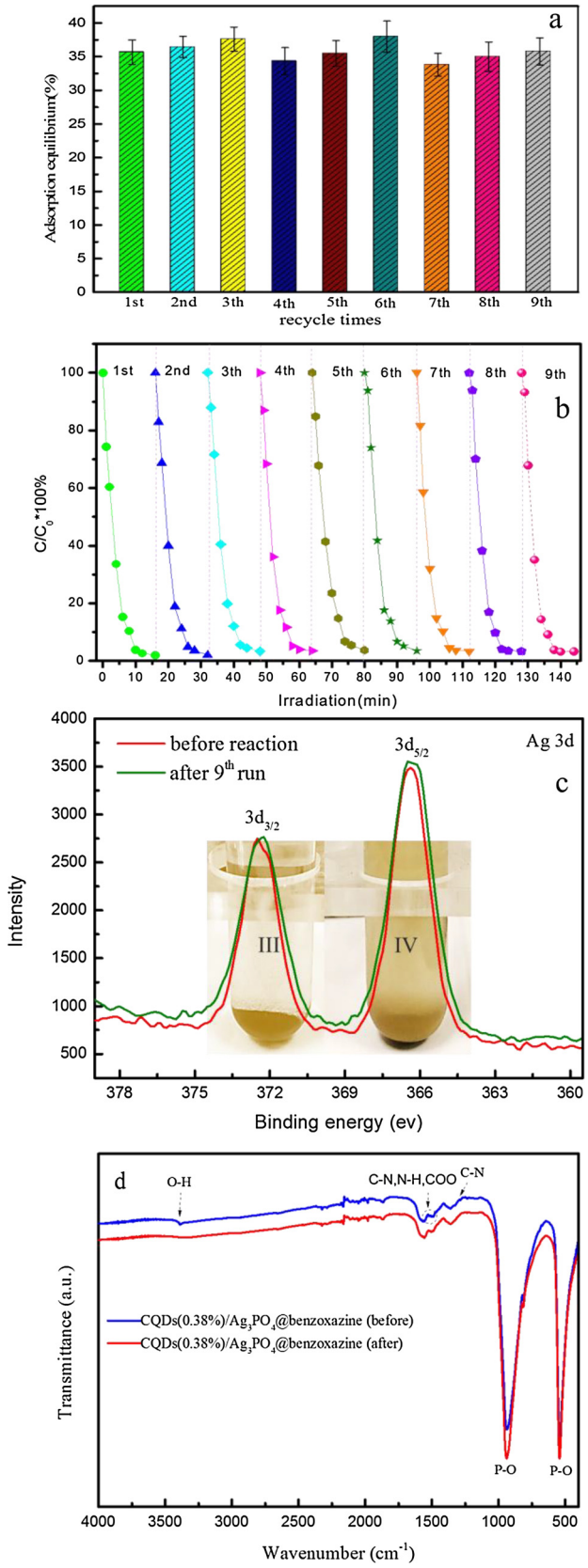

Fig. 7. (a) Equilibrium adsorption of SMX by CQDs(0.38%)/Ag_3PO_4@benzoxazine under dark stir for 30 min during every recycling catalytic process; (b) Cycling runs of CQDs(0.38%)/Ag_3PO_4@benzoxazine for SMX photodegradation; (c) Ag 3d XPS spectra of CQDs(0.38%)/Ag_3PO_4@benzoxazine before and after 9th recycling runs [inset (III) and (IV) show the color of CQDs(0.38%)/Ag_3PO_4@benzoxazine before and after 9th cycling runs of photodegradation SMX, (d) FT-IR spectrum of CQDs(0.38%)/Ag_3PO_4@benzoxazine before and after 9th recycling use. (For interpretation of the references to colour in the text, the reader is referred to the web version of this article.)

anti-photocorrosion. Even after 9th cycles, more than 96% of SMX could be photodegraded within 15 min (Fig. 7b). Moreover, XPS peaks of Ag $3d_{5/2}$ and $3d_{3/2}$ of Ag^+ (Ag_3PO_4 tetrapods) show no obvious shifts after photocatalytic reaction, which further confirm the valence states of sliver in composite are unchanged. Meanwhile, the color (yellow) of CQDs(0.38%)/Ag_3PO_4@benzoxazine composite (insite III, IV of Fig. 7c) did not change after photocatalytic degradation also supposed that the Ag^+ was unreduced. In addition, the FT-IR analysis of CQDs(0.38%)/Ag_3PO_4@benzoxazine before and after 9th recycling runs was comparatively studied. As shown in Fig. 7d, both the partial absorption peaks (C—N, N—H,COO) of benzoxazine and CQDs and the typical absorption peaks of Ag_3PO_4 were observed. As expected, the position of absorption peaks of CQDs(0.38%)/Ag_3PO_4@benzoxazine before and after recycling runs have no shift, further confirming the stability of benzoxazine and CQDS in the whole recycling photocatalytic process. Thus, CQDs(0.38%)/Ag_3PO_4@benzoxazine composite not only accelerated the generation of charge carriers but also inhibit the photocorrosion of Ag_3PO_4 tetrapods via promoting the migration of photogenerated electrons in the core-shell structure.

3.4. Possible degradation pathway of SMX

The intermediate products during the photocatalytic degradation process are identified by LC–MS/TOF, and iron spectra at different retention time (RT) of SMX photodegradation sample before and after (4, 8, 12 and 16 min) are presented in ESI Scan (Supplementary material Fig. S2). Typical ions spectra {m/z = 254 ($[M+H]^+$)} of SMX at RT = 9.891 min was detected in original solution. After visible light irradiation, nine ions spectra at RT = 4.154–12.869 min was detected. These main product ions at m/z = 218 ($[M+H]^+$), m/z = 202 ($[M+H]^+$), m/z = 179 ($[M+H]^+$), m/z = 165 ($[M+H]^+$), m/z = 156 ($[M+H]^+$), m/z = 148 ($[M+H]^+$), m/z = 120 ($[M+H]^+$), m/z = 107 ($[M+H]^+$) and m/z = 99 ($[M+H]^+$) might be identified as $C_7H_9N_2O_4S$, $C_7H_9N_2O_3S$, $C_4H_4NO_5S$, $C_4H_6NO_4S$, $C_6H_5NO_2S$, $C_4H_5NO_3S$, $C_3H_5NO_2S$, $C_2H_4NO_2S$ and $C_4H_6N_2O$. Based on the electron cloud density of SMX by Gaussian calculation and previous literatures [59,61–67], the possible photocatalytic degradation pathways of SMX are proposed and shown in Scheme 2.

3.5. Proposed mechanism

In order to further investigate the photocatalytic degradation mechanism, the free radicals trapping experiments of CQDs(0.38%)/Ag_3PO_4@benzoxazine composite were conducted to determine the main reactive species (Fig. 8). In the process of photodegradation dyes (MB and RhB solution), the hole (h^+) scavenger [ethylenediamine tetraacetic acid disodium salt (EDTA-2Na)], hydroxyl radical (·OH) scavenger [tert-butanol] and superoxide radical scavenger (·O_2) [p-benzoquinone] were added in. It is found that EDTA-2Na significantly inhibits the catalytic activity of CQDs(0.38%)/Ag_3PO_4@benzoxazine, resulting in a low removal rate of dyes. On the contrary, although adding tert-butanol shows slight influence on the removal of RhB, photocatalytic degradation of MO was almost not affected. Similarly, addition of p-benzoquinone had a negligible effect on the photodegradation MO and RhB. Such different influence by EDTA-2Na, tert-butanol and p-benzoquinone suggested that the holes photoinduced were the main active oxidizing species which played the dominant role in the photocatalytic process. Based on the above research, the possible photocatalytic degradation mechanism of CQDs(0.38%)/Ag_3PO_4@

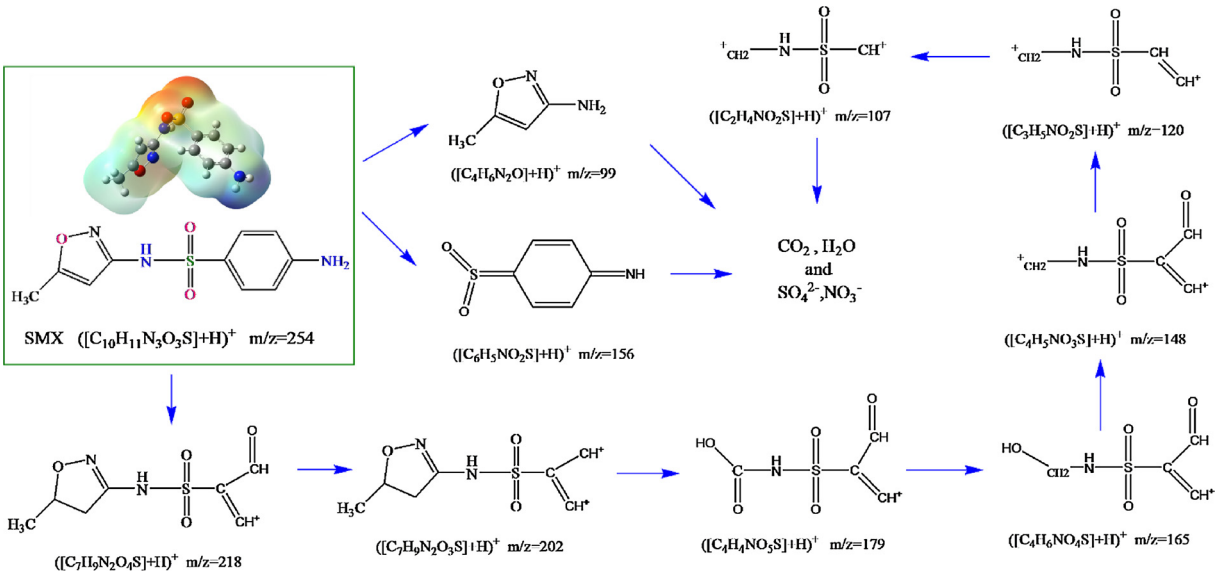

Scheme 2. Proposed photodegradation pathways of SMX over CQDs(0.38%)/Ag_3PO_4@benzoxazine.

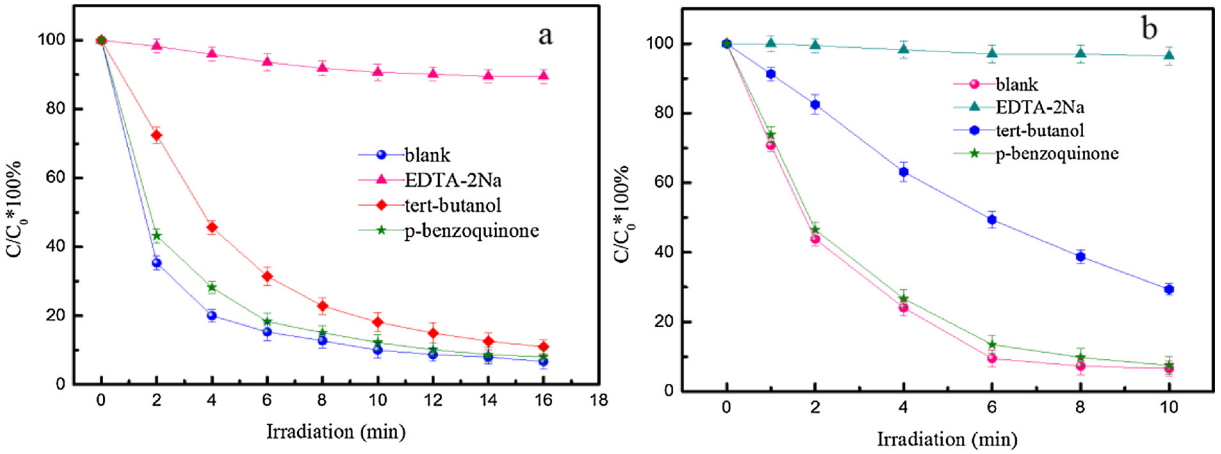

Fig. 8. Plots of photogenerated active species trapped in the system during photodegradation of MO (a) and RhB (b) over CQDs(0.38%)/Ag_3PO_4@benzoxazine.

benzoxazine is proposed. As shown in Scheme 3, due to its electron acceptor/donor characteristic, CQDs act as the 'exciter' which can induce more photocarrier generation via strengthening light absorption and energy conversion by UPCL effect. Meanwhile, CQDs can accelerate the transfer of electrons from conduction band of Ag_3PO_4 tetrapods to the bottom of conduction band of CQDs. On the other hand, the electrons flow into silver amine complex compound which acted as the bridge between core and shell, and then accompanied by series of free radical chain reaction which reduced OH^- or O_2 to '$\cdot HO_2$', '$\cdot O_2$' in solution. Actually, since abundant of CQDs are decorated on benzoxazine shell, these two electrons flow pathways mentioned above existed simultaneously and hindered the recombination of electron-hole pairs. More importantly, the h^+ isolated could oxidize the organic pollutants and OH- effectively. Thus, CQDs(0.38%)/Ag_3PO_4@benzoxazine exhibited excellent photocatalytic activity and anti-photocorrosion capability (Figs. 6 and 7).

4. Conclusions

Novel 3D core-shell CQDs(0.38%)/Ag_3PO_4@benzoxazine composites with more {110} facets exposed were successively synthesized through electrochemical oxidation, chemical precipitation and molecular self-assembly reaction. In CQDs/Ag_3PO_4@benzoxazine composite, CQDs act as an 'exciter' which can not only activate more photocarrier generation from high-energy facets of Ag_3PO_4 tetrapods via UPCL effect, but also accelerate the electrons transfer from CB of Ag_3PO_4 tetrapods to the bottom of CB of CQDs. On the other hand, the electrons flow into silver amine complex compound which acted as the bridge between core and shell, and then accompanied by series of free radical chain reaction which reduced H_2O or O_2 to $\cdot HO_2$, $\cdot O_2$ in solution. In addition, the 3D core-shell structure effectively decreased the solubility of Ag_3PO_4. Thus, 3D core-shell CQDs(0.38%)/Ag_3PO_4@benzoxazine exhibited excellent photocatalytic activity and anti-photocorrosion property. Furthermore, the intermediate products and possible degradation pathway of SMX were proposed. In summary, this study has not only prepared a promising visible-light responses photocatalyst which could be used in environment remediation and purification processes, but also provided a simple and efficient way to improve the photocatalytic activity and anti-photocorrosion of Ag_3PO_4.

Acknowledgements

This research was supported by Water Resource Research Project of Jiangsu Province (2016039), the Fundamental Research Funds for the Central Universities (0211-14380065) and the State Key Program of National Natural Science of China (No. 51438008).

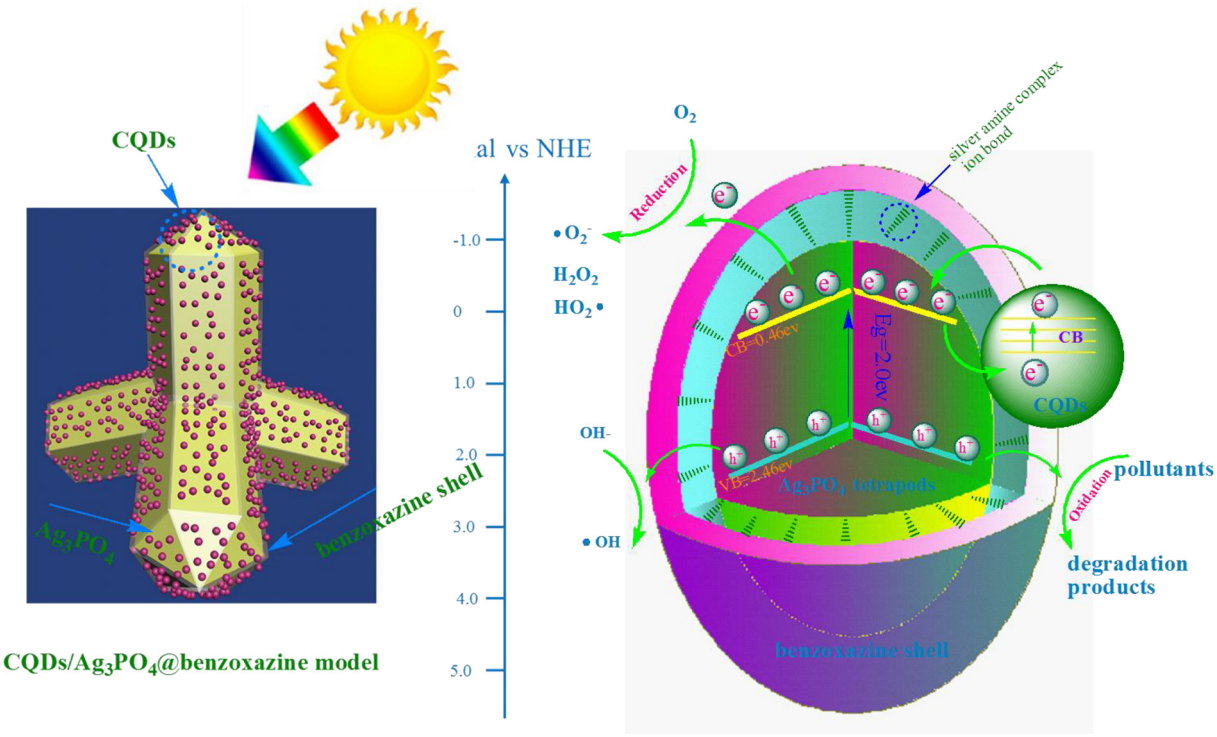

Scheme 3. Schematic illustration of the energy band structure of the 3D CQDs(0.38%)/Ag_3PO_4@benzoxazine composites and the proposed charge mechanism.

Appendix A. Supplementary data

Supplementary material related to this article can be found, in the online version, at doi:https://doi.org/10.1016/j.apcatb.2018.03.085.

References

[1] C. Tang, E. Liu, J. Wan, X. Hu, J. Fan, Appl. Catal. B: Environ. 181 (2016) 707–715.
[2] L. Wang, Y. Chai, J. Ren, J. Ding, Q. Liu, W.L. Dai, Dalton Trans. 44 (2015) 14625–14634.
[3] Y. Chang, K. Yu, C. Zhang, R. Li, P. Zhao, L.-L. Lou, S. Liu, Appl. Catal. B: Environ. 176–177 (2015) 363–373.
[4] S. Shen, L. Guo, X. Chen, F. Ren, S.S. Mao, Int. J. Hydrogen Energy 35 (2010) 7110–7115.
[5] S.-P. Hu, C.-Y. Xu, W.-S. Wang, F.-X. Ma, L. Zhen, Ceram. Int. 40 (2014) 11689–11698.
[6] N. Wetchakun, S. Chaiwichain, B. Inceesungvorn, K. Pingmuang, S. Phanichphant, A.I. Minett, J. Chen, ACS Appl. Mater. Interfaces 4 (2012) 3718–3723.
[7] Y.-X. Zhou, L. Tong, X.-H. Zeng, X.-B. Chen, New J. Chem. 38 (2014) 1973–1979.
[8] Q. Hao, R. Wang, H. Lu, Ca. Xie, W. Ao, D. Chen, C. Ma, W. Yao, Y. Zhu, Appl. Catal. B: Environ. 219 (2017) 63–72.
[9] S. Luo, J. Ke, M. Yuan, Q. Zhang, P. Xie, L. Deng, S. Wang, Appl. Catal. B: Environ. 221 (2018) 215–222.
[10] J. Xiao, W. Yang, Q. Li, Appl. Catal. B: Environ. 218 (2017) 111–118.
[11] H. Li, L. Shen, K. Zhang, B. Sun, L. Ren, P. Qiao, K. Pan, L. Wang, W. Zhou, Appl. Catal. B: Environ. 220 (2018) 111–117.
[12] M. Chen, J. Ma, B. Zhang, F. Wang, Y. Li, C. Zhang, H. He, Appl. Catal. B: Environ. 223 (2018) 209–215.
[13] Y. Bi, S. Ouyang, N. Umezawa, J. Cao, J. Ye, J. Am. Chem. Soc. 133 (2011) 6490–6492.
[14] H. Wang, Y. Bai, J. Yang, X. Lang, J. Li, L. Guo, Chemistry 18 (2012) 5524–5529.
[15] L. Liu, Y. Qi, J. Lu, S. Lin, W. An, Y. Liang, W. Cui, Appl. Catal. B: Environ. 183 (2016) 133–141.
[16] H. Tong, S. Ouyang, Y. Bi, N. Umezawa, M. Oshikiri, J. Ye, Adv. Mater. 24 (2012) 229–251.
[17] Z. Yi, J. Ye, N. Kikugawa, T. Kako, S. Ouyang, H. Stuart-Williams, H. Yang, J. Cao, W. Luo, Z. Li, Y. Liu, R.L. Withers, Nat. Mater. 9 (2010) 559–564.
[18] Y. Bi, H. Hu, S. Ouyang, G. Lu, J. Cao, J. Ye, Chem. Commun. (Camb.) 48 (2012) 3748–3750.
[19] J. Wang, F. Teng, M. Chen, J. Xu, Y. Song, X. Zhou, CrystEngComm 15 (2013) 39–42.
[20] M. Li, M. Chen, J. Wang, F. Teng, CrystEngComm 16 (2014) 1237–1240.
[21] X. Hua, Y. Jin, K. Wang, N. Li, H. Liu, M. Chen, S. Paul, Y. Zhang, X. Zhao, F. Teng, Catal. Commun. 52 (2014) 49–52.
[22] K. Wang, J. Xu, X. Hua, N. Li, M. Chen, F. Teng, Y. Zhu, W. Yao, J. Mol. Catal. A: Chem. 393 (2014) 302–308.
[23] L. Wang, N. Li, Q. Zhang, S. Lou, Y. Zhao, M. Chen, F. Teng, CrystEngComm 16 (2014) 9326–9330.
[24] C. Zhu, L. Zhang, B. Jiang, J. Zheng, P. Hu, S. Li, M. Wu, W. Wu, Appl. Surf. Sci. 377 (2016) 99–108.
[25] P. Tan, X. Chen, L. Wu, Y.Y. Shang, W. Liu, J. Pan, X. Xiong, Appl. Catal. B: Environ. 202 (2017) 326–334.
[26] X. Li, T. Wan, J. Qiu, H. Wei, F. Qin, Y. Wang, Y. Liao, Z. Huang, X. Tan, Appl. Catal. B: Environ. 217 (2017) 591–602.
[27] C. Mu, Y. Zhang, W. Cui, Y. Liang, Y. Zhu, Appl. Catal. B: Environ. 212 (2017) 41–49.
[28] N. Shao, J. Wang, D. Wang, P. Corvini, Appl. Catal. B: Environ. 203 (2017) 964–978.
[29] C. Yuan, B. Liu, F. Liu, M.Y. Han, Z. Zhang, Anal. Chem. 86 (2014) 1123–1130.
[30] X. Wang, L. Cao, F. Lu, M.J. Meziani, H. Li, G. Qi, B. Zhou, B.A. Harruff, F. Kermarrec, Y.P. Sun, Chem. Commun. (Camb.) (2009) 3774–3776.
[31] Y. Li, Y. Hu, Y. Zhao, G. Shi, L. Deng, Y. Hou, L. Qu, Adv. Mater. 23 (2011) 776–780.
[32] Y. He, L. Zhang, B. Teng, M. Fan, Environ. Sci. Technol. 49 (2015) 649–656.
[33] M. Shaban, M.R. Abukhadra, A. Hamd, R.R. Amin, A. Abdel Khalek, J. Environ. Manage. 204 (2017) 189–199.
[34] X. Li, W. Zhang, W. Cui, Y. Sun, G. Jiang, Y. Zhang, H. Huang, F. Dong, Appl. Catal. B: Environ. 221 (2018) 482–489.
[35] F. Chen, W. An, L. Liu, Y. Liang, W. Cui, Appl. Catal. B: Environ. 217 (2017) 65–80.
[36] Y. Liang, S. Lin, L. Liu, J. Hu, W. Cui, Appl. Catal. B: Environ. 164 (2015) 192–203.
[37] L. Liu, L. Ding, Y. Liu, W. An, S. Lin, Y. Liang, W. Cui, Appl. Catal. B: Environ. 201 (2017) 92–104.
[38] J.Y. Sun, X. Zhao, W.R. Illeperuma, O. Chaudhuri, K.H. Oh, D.J. Mooney, J.J. Vlassak, Z. Suo, Nature 489 (2012) 133–136.
[39] P. Calvert, Adv. Mater. 21 (2009) 743–756.
[40] Y. Hu, S. Huang, X. Zheng, F. Cao, T. Yu, G. Zhang, Z. Xiao, J. Liang, Y. Zhang, RSC Adv. 6 (2016) 62244–62251.
[41] C. Gonzalez-Rodriguez, J.R. Suarez, J.A. Varela, C. Saa, Angew. Chem. Int. Ed. Engl. 54 (2015) 2724–2728.
[42] S. Wang, W.C. Li, G.P. Hao, Y. Hao, Q. Sun, X.Q. Zhang, A.H. Lu, J. Am. Chem. Soc. 133 (2011) 15304–15307.
[43] C.-Y. Hui, Y.Y. Lin, F.-C. Chuang, K.R. Shull, W.-C. Lin, J. Polym. Sci. Part B: Polym. Phys. 44 (2006) 359–370.
[44] M. Liu, Y. Xu, F. Niu, J.J. Gooding, J. Liu, The Analyst 141 (2016) 2657–2664.
[45] D. Tang, H. Zhang, H. Huang, R. Liu, Y. Han, Y. Liu, C. Tong, Z. Kang, Dalton Trans. 42 (2013) 6285–6289.
[46] R. Wang, K.-Q. Lu, Z.-R. Tang, Y.-J. Xu, J. Mater. Chem. A 5 (2017) 3717–3734.
[47] P. Dong, Y. Wang, B. Cao, S. Xin, L. Guo, J. Zhang, F. Li, Appl. Catal. B: Environ. 132–133 (2013) 45–53.
[48] Hamerton, K. Ennis, B.J. Howlin, L.T. McNamara, React. Funct. Polym. 73 (2013) 1612–1624.
[49] X. Ma, H. Li, Y. Wang, H. Li, B. Liu, S. Yin, T. Sato, Appl. Catal. B: Environ. 158–159 (2014) 314–320.
[50] X. Yang, J. Qin, Y. Jiang, K. Chen, X. Yan, D. Zhang, R. Li, H. Tang, Appl. Catal. B:

Environ. 166–167 (2015) 231–240.
[51] S. Liu, H. Sun, K. O'Donnell, H.M. Ang, M.O. Tade, S. Wang, J. Colloid Interface Sci. 464 (2016) 10–17.
[52] Y. Bu, Z. Chen, C. Sun, Appl. Catal. B: Environ. 179 (2015) 363–371.
[53] H. Li, Z. Kang, Y. Liu, S.-T. Lee, J. Mater. Chem. 22 (2012) 24230.
[54] Y. Lv, K. Huang, W. Zhang, B. Yang, F. Chi, S. Ran, X. Liu, Ceram. Int. 40 (2014) 8087–8092.
[55] P. Chen, F. Wang, Z.-F. Chen, Q. Zhang, Y. Su, L. Shen, K. Yao, Y. Liu, Z. Cai, W. Lv, G. Liu, Appl. Catal. B: Environ. 204 (2017) 250–259.
[56] Q. Li, Q. Tang, N. Du, Y. Qin, J. Xiao, B. He, H. Chen, L. Chu, J. Power Sources 248 (2014) 816–821.
[57] H. Wang, Y. Liang, L. Liu, J. Hu, P. Wu, W. Cui, Appl. Catal. B: Environ. 208 (2017) 22–34.
[58] Y. Zhang, W. Cui, W. An, L. Liu, Y. Liang, Y. Zhu, Appl. Catal. B: Environ. 221 (2018) 36–46.
[59] Q. Cai, J. Hu, J. Hazard. Mater. 323 (2017) 527–536.
[60] Y. Song, J. Tian, S. Gao, P. Shao, J. Qi, F. Cui, Appl. Catal. B: Environ. 210 (2017) 88–96.
[61] M.G. Peleyeju, E.H. Umukoro, L. Tshwenya, R. Moutloali, J.O. Babalola, O.A. Arotiba, RSC Adv. 7 (2017) 40571–40580.
[62] L. Zhou, W. Zhang, L. Chen, H. Deng, J. Colloid Interface Sci. 487 (2017) 410–417.
[63] Y. Bao, T.T. Lim, Z. Zhong, R. Wang, X. Hu, J. Colloid Interface Sci. 505 (2017) 489–499.
[64] S. Hussain, J.R. Steter, S. Gul, A.J. Motheo, J. Environ. Manage. 201 (2017) 153–162.
[65] J. Yang, Z. Li, H. Zhu, Appl. Catal. B: Environ. 217 (2017) 603–614.
[66] H. Zhang, Z. Wang, R. Li, J. Guo, Y. Li, J. Zhu, X. Xie, Chemosphere 185 (2017) 351–360.
[67] W. Zhu, F. Sun, R. Goei, Y. Zhou, Appl. Catal. B: Environ. 207 (2017) 93–102.